Chemical Physics Letters 614 (2014) 136–142

Contents lists available at ScienceDirect

Chemical Physics Letters

journal homepage: www.elsevier.com/locate/cplett

Description of pnicogen bonding with the help of vibrational spectroscopy—The missing link between theory and experiment

D. Setiawan, E. Kraka, D. Cremer*

Department of Chemistry, Southern Methodist University, 3215 Daniel Avenue, Dallas, TX 75275, United States

ARTICLE INFO

Article history:
Received 15 August 2014
In final form 9 September 2014
Available online 17 September 2014

ABSTRACT

The nature of the E···E′ pnicogen bond (E = N, P, As) in dimers such as $H_2FP\cdots PH_2F$ (**1**) and $H_3N\cdots PHNO_2$ (**2**) can be described using vibrational spectroscopy in form of the calculated infrared and depolarized Raman scattering spectra. Utilizing the six calculated intermonomer frequencies, the corresponding local mode E···E′ stretching frequency and force constant are obtained, where the latter provides a unique measure of the E···E′ bond strength. Pnicogen bonding in **1** is relative strong (bond strength order n = 0.151) and covalent whereas pnicogen bonding in **2** is electrostatic (n = 0.047) because of a different bonding mechanism.

1. Introduction

In the last years, pnicogen bonding between two monomers ER_3 leading to dimers $R_3E\cdots E'R'_3$ (E, E′: N, P, As; R, R′: H, halogen, alkyl, etc.) has been intensively investigated where most of the work has been based on quantum chemical calculations [1–11]. Only scattered experimental results based on X-ray diffraction [12] and NMR measurements [13] could be reported providing more or less indirect or incomplete information on pnicogen interactions of the type E···E′. There is a pressing need to identify and characterize pnicogen bonding more directly utilizing modern spectroscopic methods. Terahertz spectroscopy [14,15] or depolarized Raman scattering [16] are promising experimental tools, which can measure vibrational frequencies down to 50 cm^{-1}. This is a prerequisite to record the intermonomer frequencies of a pnicogen-bonded dimer. If the stretching character of one of the six frequencies strongly domintes, the associated force constant is a direct measure on the strength of the pnicogen bond E···E′, which is difficult to obtain with other experimental means. The description can be improved by deriving from the measured frequencies the corresponding local mode frequencies and their force constants [17] as they provide a precise measure of the E···E′ bond strength irrespective of the composition of the original normal modes.

We will demonstrate in this work that among the intermonomer modes of pnicogen-bonded dimers the E···E′ stretching frequency can easily be detected and used to obtain the corresponding local E···E′ stretching frequency and force constant. For this purpose, we will calculate the infrared and depolarized Raman scattering spectra of the two dimers $H_2FP\cdots PH_2F$ (**1**) and $H_3N\cdots PHNO_2$ (**2**) and present a method to analyze their intermonomer E···E′ stretching frequencies for the purpose of assessing the strength and nature of the pnicogen bond. The method is a combination of the local mode analysis of Konkoli and Cremer [18] and the electron density /energy density analysis of Cremer and Kraka [19,20]. Then, we will make suggestions how these frequencies can be experimentally detected by using either depolarized Raman scattering or terahertz spectroscopy.

2. Computational methods

Binding energies, equilibrium geometries and normal vibrational frequencies of **1** and **2** were calculated using the ωB97X-D density functional [21,22]. The latter was chosen because it provides a reliable description of non-covalent interactions in cases where dispersion and other long range van der Waals interactions play an important role [23,24] and because it reproduces CCSD(T) [25] results satisfactorily, as was shown by Sherrill et al. [26]. The DFT calculations were carried out using an ultrafine grid and tight convergence criteria in the geometry optimizations to guarantee a reliable calculation of vibrational frequencies. The binding energies ΔE of the dimers **1** and **2** (calculated relative to the energies of the separated monomers at their equilibrium geometries and not including any vibrational corrections at 0 K) were corrected for basis set superposition errors employing the counterpoise method of Boys and Bernardi [27]. Free binding energies $\Delta G(T)$ were calculated at T = 298, 100 and 5 K (all at 1 atm pressure) to determine

* Corresponding author.
E-mail address: Dieter.cremer@gmail.com (D. Cremer).

http://dx.doi.org/10.1016/j.cplett.2014.09.030
0009-2614/

the temperature at which ΔG becomes negative, thus providing a chance of observing a given dimer and characterizing it by experimental means.

Dunning's aug-cc-pVTZ basis set [28] was used to describe dispersion interactions sufficiently accurately. Beside complex binding energy, geometry, and vibrational frequencies, infrared and Raman spectra including the Raman depolarization ratio ρ [16] were calculated. The local vibrational modes were derived according to Konkoli and Cremer [18,29] where the relationship between normal and local vibrational frequencies was determined with the adiabatic connection scheme (ACS) [30,31]. For each normal mode frequency the corresponding local mode and coupling frequencies were determined and checked whether they lead to the conservation of the zeropoint energy of the molecule. The local stretching force constants k_a were used to determine the relative bond strength order (BSO) n according to the relationship $n = a(k_a)^b$ where for **1** the constants a(PP) = 0.578 and b(PP) = 0.894 were obtained by giving the PP bonds in diphosphine and diphosphene n-values of 1 and 2 and requiring that for k_a = 0 the BSO value is zero [32]. In the case of **2**, aminophosphine and aminophosphene were used as references to determine a(NP) = 0.300 and b(NP) = 0.958.

For each pnicogen interaction the (3, −1) critical point $\mathbf{r}_b$ of the electron distribution $\rho(\mathbf{r})$ was determined and the energy density $H(\mathbf{r}_b) = H_b$ calculated. According to the Cremer–Kraka criterion [19,20], a negative energy density H_b indicates covalent bonding whereas a positive H_b speaks of electrostatic interactions. Local mode and electron density analysis were carried out with the program package COLOGNE 2014 [33], whereas for the DFT calculations GAUSSIAN 09 [34] was used.

3. Detection of pnicogen bonding with vibrational spectroscopy

The description of intermonomer bonding in pnicogen-dimers such as **1** or **2** is based in this work on the local vibrational mode analysis [18,29]. Vibrational modes probe the electronic structure and the bonds of a molecule or a molecular complex. Therefore, the stretching force constants provide a direct measure of the strength of the bonds of a molecule and the bending force constants about bond–bond interactions based on hybridization, electrostatic, and/or polarization effects [18,29,17,32,30,35].

However, this information can only be extracted from the calculated or measured normal mode frequencies if the coupling between the vibrational modes is suppressed and local vibrational modes are obtained [18,29,17,36]. Experimentally, this has been accomplished (at least approximately) via the *isolated stretching frequencies* of McKean [37] or the overtone spectra in the case of XH bonds [38]. A general computational solution has been found by Konkoli and Cremer [18], who showed that mode coupling includes electronic and kinematic (mass) coupling contributions. Their way of determining local vibrational modes is closely related to Wilson's solution of the vibrational problem [39]. Wilson showed that by solving the Euler–Lagrange equations the basic equation of vibrational spectroscopy is obtained [39]:

$$\mathbf{F}^q\mathbf{D} = \mathbf{G}^{-1}\mathbf{D}\boldsymbol{\Lambda} \tag{1}$$

where $\mathbf{F}^q$ is the calculated force constant matrix expressed in internal coordinates q_n, $\mathbf{D}$ collects the vibrational eigenvectors $\mathbf{d}_\mu$ in form of column vectors ($\mu = 1, \cdots, N_{vib}$ with $N_{vib} = 3N - L$; N: number of atoms; L: number of translations and rotations), $\mathbf{G}$ is the Wilson matrix for the kinetic energy [39], and $\boldsymbol{\Lambda}$ is a diagonal matrix containing the vibrational eigenvalues $\lambda_\mu = 4\pi^2c^2\omega_\mu^2$ with ω_μ presenting the vibrational frequency of mode $\mathbf{d}_\mu$. Solution of the Wilson equation implies the diagonalization of matrix $\mathbf{F}^q$ to give the diagonal matrix $\mathbf{K}$. In this way, the electronic coupling between the local modes is eliminated. Konkoli and Cremer suppress also the kinematic coupling by starting from the mass-decoupled Euler–Lagrange equations [18]. Zou and Cremer demonstrated that in this way the mass-decoupled equivalent of the Wilson equation [30,35] is obtained, which by diagonalization directly leads to the local vibrational modes $\mathbf{a}_n$ being associate with internal coordinates q_n [18,30,31,35]:

$$\mathbf{a}_n = \frac{\mathbf{K}^{-1}\mathbf{d}_n^\dagger}{\mathbf{d}_n\mathbf{K}^{-1}\mathbf{d}_n^\dagger} \tag{2}$$

Here, $\mathbf{d}_n$ is a row vector of matrix $\mathbf{D}$. The local mode force constant k_a^n for mode n is given by Eq. (3):

$$k_a^n = \mathbf{a}_n^\dagger\mathbf{K}\mathbf{a}_n \tag{3}$$

If k_a^n is a stretching force constant, it can be used to determine the BSO value n The local mode frequency ω_a^n is obtained from

$$(\omega_a^n)^2 = \frac{G_{nn}\quad k_a^n}{4\pi^2c^2} \tag{4}$$

where element G_{nn} of matrix $\mathbf{G}$ defines the local mode mass [18]. In the following, we will simplify the notation to k_a and ω_a because only the local E···E′ stretching mode is discussed here. Each local mode is associated with a specific structural unit of a molecule, which in turn can be described by a single internal coordinate: 1-bond diatomic units characterized by a bond length, 2-bond triatomic units characterized by a bond angle, etc. In this way, the local stretching, bending, or torsional force constants describe the strength of the chemical bond, the stiffness or bending (caused by hybridization, polarization, and other electrostatic effects), or the rotational barrier.

The N_{vib} normal vibrational modes are exactly defined, whereas the number of local vibrational modes L_{vib} can be significantly larger. In previous work, Cremer et al. [30,31,35] have shown that with the help of perturbation theory and a perturbation parameter λ (λ = 0: local modes; λ = 1: normal modes) the local mode vectors and their associated frequencies can be stepwise transformed into normal modes and their frequencies, which leads to the ACS between local and normal modes [30]. In this way, the kinematic coupling pattern between the modes is resolved and also those local modes are identified that have the strongest overlap with the normal modes. Starting with a set of $L_{vib} > N_{vib}$, only those local modes are maintained in the ACS for increasing λ, which strongly overlap with the normal modes. Local modes with insufficient overlap lead to zero frequency values for λ = 1.

4. Results and discussion

Homodimer **1** and heterodimer **2** are representative pnicogen-bonded dimers. For **1**, ΔE is −5.87 kcal/mol and $\Delta G(T)$ (T = 298, 100, and 5 K) 6.70, −0.72, and −3.94 kcal/mol, respectively, leading to T(obs) = 116 K, at which **1** becomes observable. For **2**, ΔE is −7.56 kcal/mol and $\Delta G(T)$ 2.10, −3.31, and −5.68 kcal/mol at 298, 100, and 5 K, respectively, suggesting T(obs) to be 221 K. Both dimers are more stable than the water dimer (ΔE = −5.0 kcal/mol [40]). The P···P distance of 2.543 Å in **1** is 1.057 Å shorter than twice the phosphorus van der Waals radius of 1.800 Å [41]. The PF bonds (1.626 Å) are 0.007 Å longer than in the PH_2F monomer. The N···P distance of 2.658 Å in **2** is 0.69 Å shorter than the sum of the N van der Waals radius (1.55 Å) and that of P (1.800 Å). The PN(O_2) bond (1.866 Å) is 0.023 Å longer than in the PH_2NO_2 monomer. While in the case of **1** the anti form is the most stable one, **2** adopts a syn form. This shows that obviously different electronic features contribute to the dimer stabilities. (Supporting Information available from authors)

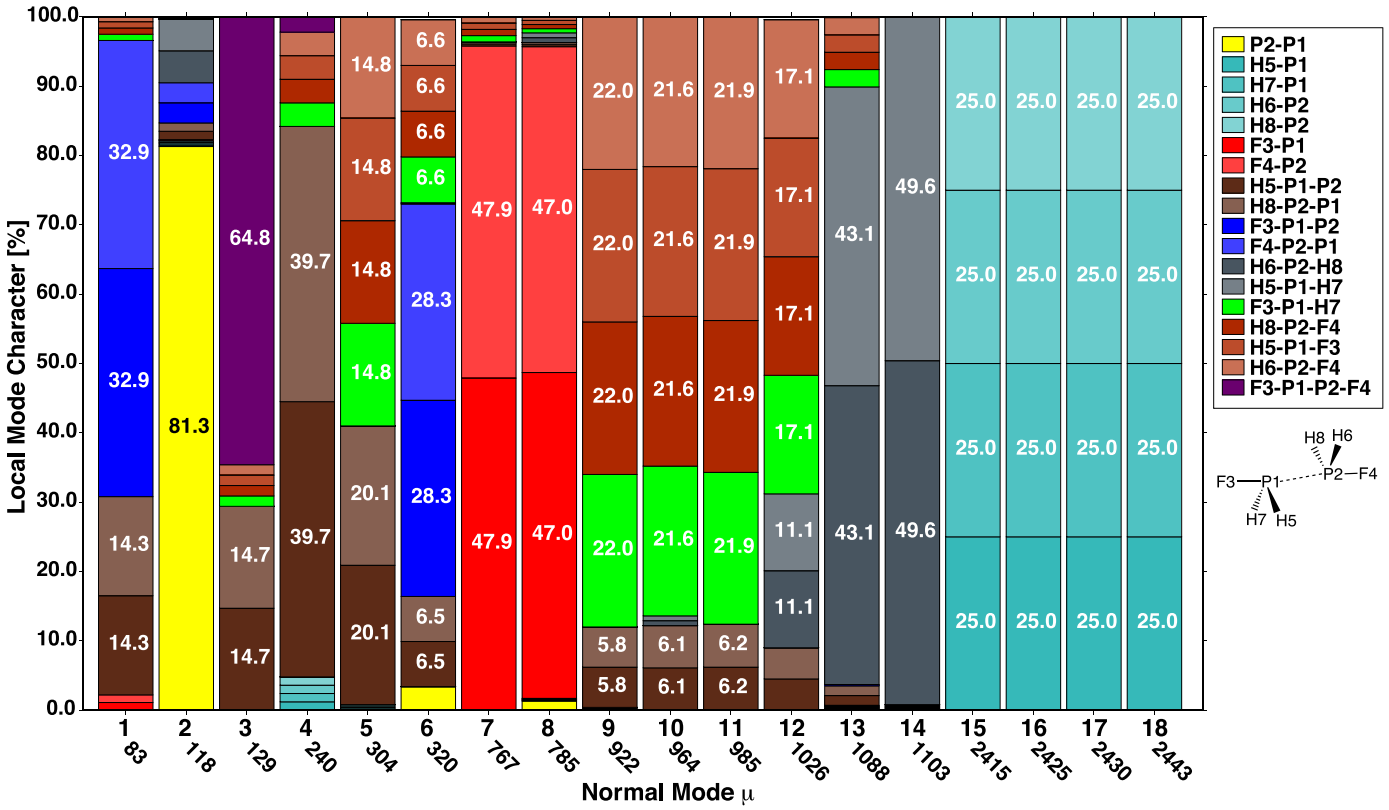

Fig. 1. Normal mode decomposition into local vibrational modes for molecule **1** shown in form of a bar diagram. The local mode contributions are color-coded according to the list given on the right side. They are given for each of the 18 normal modes where the numbering and calculated frequency of the latter are shown at the bottom of each bar. Contributions are given in percentage if larger than 5%. (For interpretation of the references to color in this figure legend, the reader is referred to the web version of this article.)

In Figure 1, the decomposition of the 18 normal vibrational modes $\mathbf{d}_\mu$ of **1** into local modes defined by set of 18 color-coded internal coordinates is presented in form of a bar diagram [29]. In Table 1, normal and local mode properties of **1** are listed. The 18 internal coordinates of the C_{2h}-symmetrical dimer **1** comprise the 6 bond lengths, the P···P interaction distance, and the FPPF dihedral angle. The remaining 10 internal coordinates are bending angles that split up into 6 intramonomer angles of the type XPY (X,Y = H or F) and 4 intermonomer angles of the type HP···P and FP···P. The associated local modes provide the largest overlap with the 18 normal modes. Redundant sets, which contain additional local modes being associated with

Table 1
Relationship between the normal and local vibrational modes of **1**.[a]

μ	Sym.	ω_μ [cm^{-1}]	m	Internal coordinate	k_a [mdyn Å^{-1}]	ω_a [cm^{-1}]	ω_{coup} [cm^{-1}]
18	A_u	2443	4	H6-P2	3.361	2418	25
17	B_g	2430	5	H8-P2	3.361	2418	12
16	B_u	2425	2	H5-P1	3.361	2418	7
15	A_g	2415	3	H7-P1	3.361	2418	−3
14	B_u	1103	13	H5-P1-H7	0.638	1055	48
13	A_g	1088	12	H6-P2-H8	0.638	1055	33
12	A_g	1026	14	H7-P1-F3	0.886	908	118
11	B_g	985	17	H6-P2-F4	0.886	908	77
10	B_u	964	16	H5-P1-F3	0.886	908	56
9	A_u	922	15	H8-P2-F4	0.886	908	14
8	A_g	785	7	F4-P2	4.065	765	20
7	B_u	767	6	F3-P1	4.065	765	2
6	A_g	320	10	F3-P1···P2	0.225	148	172
5	B_g	304	9	H8-P2···P1	0.285	503	−199
4	A_u	240	8	H5-P1···P2	0.285	503	−263
3	A_u	129	18	F3-P1···P2-F4	0.013	134	−5
2	A_g	118	1	P2···P1	0.222	156	−38
1	B_u	83	11	F4-P2···P1	0.225	148	−65
ZPE [kcal/mol]:		26.51				25.91	0.61

[a] Normal modes μ, their symmetry (Sym.), and vibrational frequencies ω_μ are given. For each local mode m, the internal coordinate driving the mode, the local stretching, bending, or torsional force constant k_a, the local frequency ω_a, and the coupling frequency ω_{coup} are listed. Bending and torsional force constants are given in mdyn Å/rad^2. The coupling frequencies are checked by calculating the zeropoint energy (ZPE): the sum of the *local mode* and *coupling mode* ZPE-contributions must be equal to the *normal mode* ZPE.

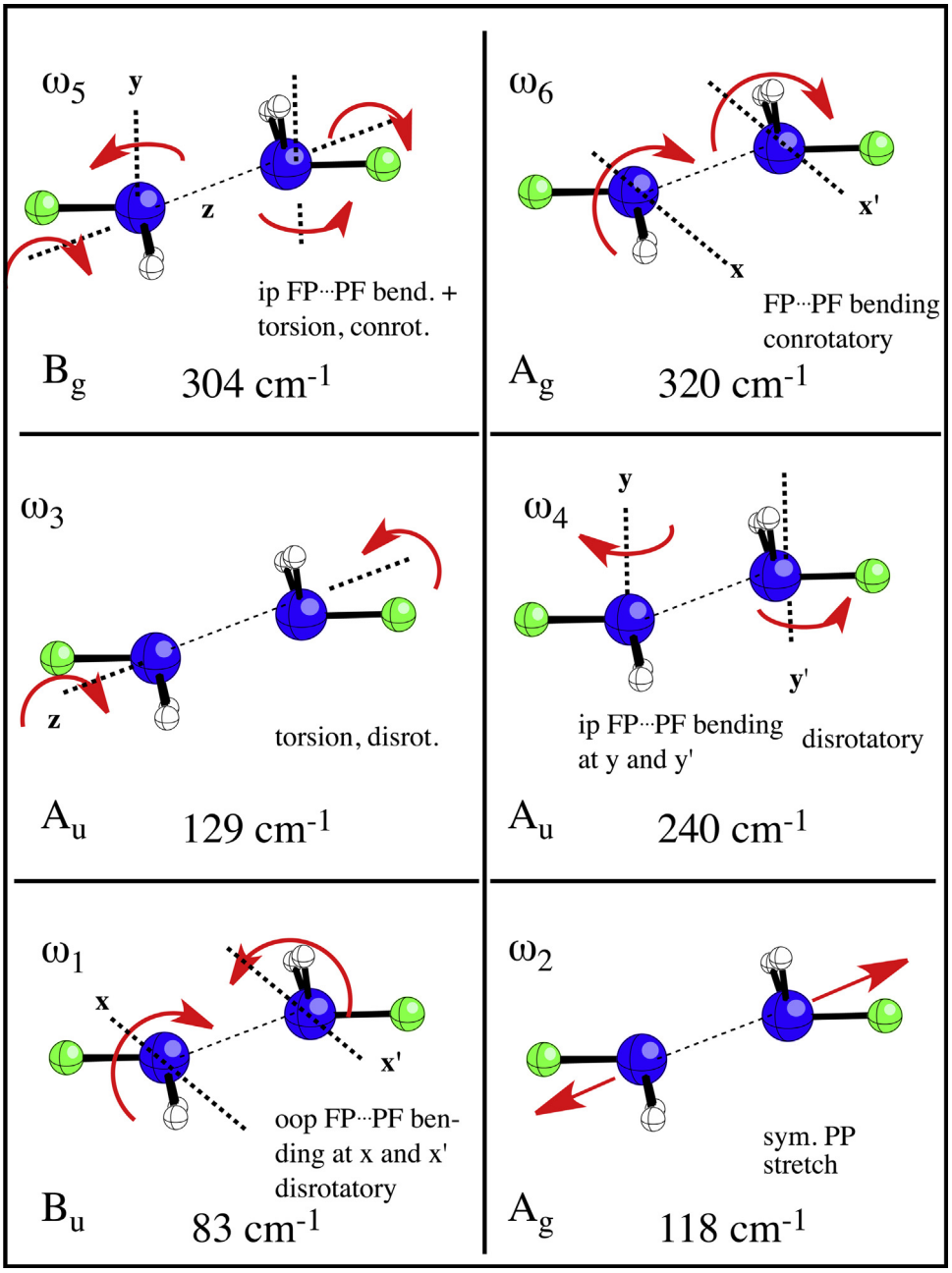

Fig. 2. The six intermonomer modes ω_1 - ω_6 of **1**. Abbreviations ip, oop, and rot denote in-plane, out-of-plane, and rotation. Frequencies from ωB97XD/aug-cc-pVTZ calculations. Note that there are 12 translations and rotations possible with regard to the principle axes of the monomers of the pnicogen complex where always pairs of opposite or equally directed translations and conrotatory or disrotatory rotations have to be considered.

additional internal coordinates were reduced by the ACS to 18 local modes.

The bar diagram in Figure 1 shows that normal mode 2 (118 cm^{-1}) contains 81% of pnicogen-pnicogen stretching character (yellow part of the bar) suggesting that this is weaker than the H-bond stretching frequency in the water dimer (normal: 143; local: 390 cm^{-1}) [40]. There are 4 PH stretching modes (15–18), the 2 PF stretching modes (7,8) and the 6 monomer bending modes (9–14) where each of these normal modes is a combination of at least 4 local modes with varying contributions. Of special interest are the 6 modes with the lowest frequencies because they correspond to the intermonomer vibrations (see Figure 2), which can provide detailed information about pnicogen bonding. The A_g-symmetrical mode 2 at 118 cm^{-1} is mixed with monomer bending (grey color) and the intermonomer bending modes FP···P (blue, Figure 1). Mode 3 is a torsional vibration of A_u-symmetry dominated by the FP···PF local mode (65%, 129 cm^{-1}, purple in Figure 1; see also Figure 2).

The other 4 intermonomer modes (1, 4, 5, and 6) correspond to the coupled in-plane (ip) or out-of-plane (oop) bending modes where the mean plane of FPPF is used as the reference plane (in the following, we will continue to use the notation ip and oop with regard to this reference plane). The oop-modes 1 at 83 cm^{-1} and 6 at 320 cm^{-1} (Figure 2) with B_u- and B_g-symmetry possess distinct FP···P bending character (Figure 1). The ip/oop modes 4 and 5 of A_u- and B_g-symmetry at 240 and 304 cm^{-1}, respectively, cannot be characterized by just one internal coordinate mode. Generally, for all modes, which involve a complex con- or disrotatory movement of two monomers relative to each other, local modes based on symmetry coordinates [42] are more appropriate. This is revealed

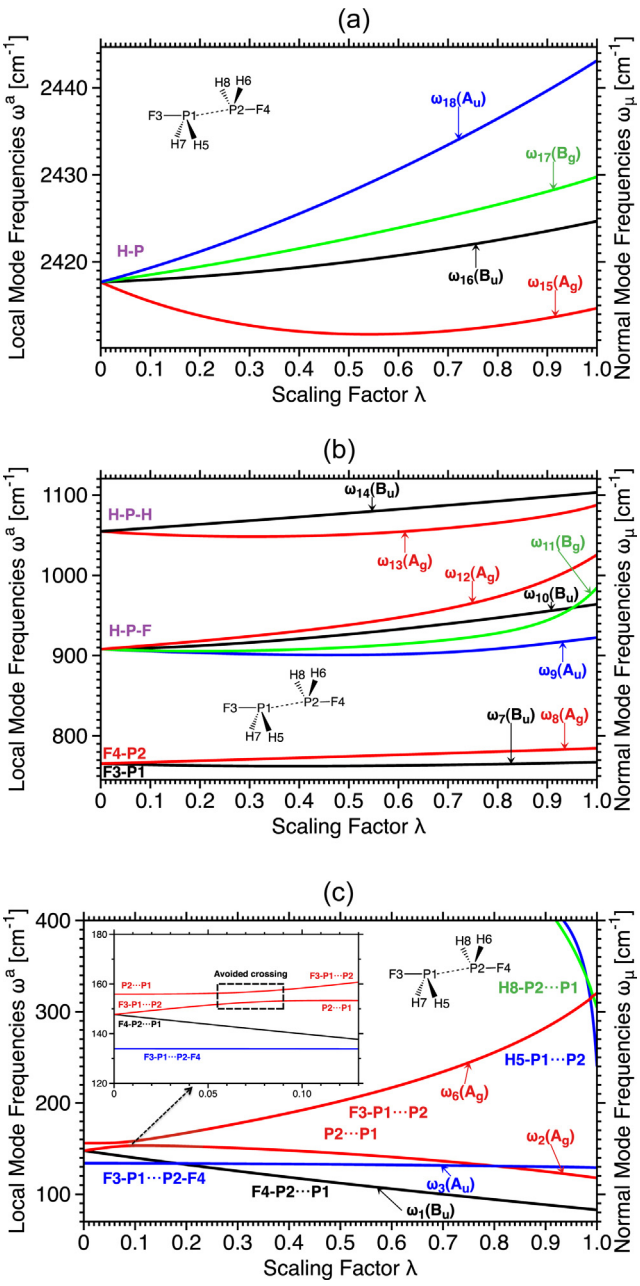

Fig. 3. Adiabatic connection scheme (ACS) of molecule **1** relating local mode frequencies (left) to normal mode frequencies ω_μ (right, compare with Table 1). Figures **a, b**, and **c** show the upper, intermediate, and lower frequency ranges, respectively. The inset in Figure **c** shows the magnified avoided crossing (AC) region between the A_g-symmetrical P···P stretching and FP···P bending modes. Different symmetries are color-coded. Local mode frequencies ω_4 and ω_5 are not shown. (For interpretation of the references to color in this figure legend, the reader is referred to the web version of this article.)

by the bar diagram in Figure 1 especially in the case of normal mode 5.

The ACS diagram of **1** is given in Figure 3(a) (high frequency range), (b) (intermediate frequency range), and (c) (low frequency range). The 4 PH stretching modes have the same local mode frequency value (2418 cm^{-1}, Table 1). They combine to 4 normal modes where mass-coupling leads to a splitting of the frequencies over a range of just 30 cm^{-1} (Table 1 and Figure 3(c)) thus indicating that the kinematic coupling of the PH stretching modes is weak because of the pyramidal PH bond arrangement enclosing HPH angles of 96° (the coupling is zero for a 90°-HPH angle). The symmetric A_g-combination adopts the smallest and the A_u-combination the highest frequency. The coupling is stronger for combinations of intramonomer HPH and HPF bending modes (ω_μ: 922 - 1103 cm^{-1}, ω_a: 908, 1055 cm^{-1}, Figure 3(b)). The local PF stretching frequencies are at 765 cm^{-1}, which have a coupling splitting of just 2 cm^{-1} (Table 1).

The important information on pnicogen bonding is contained in the low frequency range of the vibrational spectrum of **1**. The local pnicogen stretching frequency is at 156 cm^{-1} corresponding to a local stretching force constant of 0.222 mdyn/Å. An avoided crossing (AC; insert in Figure 3(c) with the A_g-symmetrical FP···P bending mode at λ = 0.06 leads to a mixing and an exchange of the character of the two modes: The lower mode continues with dominant P···P character (leading to mode 2 at 118 cm^{-1}) whereas the upper mode has dominant FP···P character and after two allowed crossings becomes the conrotatory ip-bending mode 6 at 320 cm^{-1} (Figure 2). The ACS diagram clarifies that normal mode 2 relates to the local P···P stretching mode and has to be measured in the far infrared to get a direct insight into pnicogen bonding. The local HP···P bending modes appear at 503 cm^{-1} with a bending force constant of 0.285 mdyn Å/rad^2 comparable in magnitude to the local P···P stretching force constant (0.222 mdyn/Å, Table 1), which indicates that a reorientation of the lp(P) orbital by HP···P bending significantly changes pnicogen bonding.

As shown above for **1** (Figure 1 and Table 1), the intermonomer E···E′ stretching mode should be used for the experimental identification of pnicogen-bonded complexes. This mode appears between 30 and 155 cm^{-1}. Since **1** possesses C_{2h} symmetry and normal mode 2 is of A_g symmetry (Table 1), the pnicogen stretching mode is infrared inactive according to the selection rules [16]. The calculated Raman spectrum of **1** (Figure 4) reveals that the intensity of frequency ω_2 (shown in red) is too small to be a useful test-probe. The intensities of the other two Raman active intermonomer bands ω_5 and ω_6 are also too small. Additional information can be obtained from the polarization of the Raman scattered light. The orientation of polarization is measured using a plane-polarized laser excitation and a polarizer measuring the intensity of Raman scattered light parallel and perpendicular to the polarization plane. Then, the Raman depolarization ratio ρ is calculated as the intensity ratio $I_{perpendicular}/I_{parallel}$ [16]. Symmetric vibrations give rise to polarized or partially polarized Raman lines whereas non-symmetric molecules give depolarized lines. Applying Placzek's polarizability approximation [43], the depolarization ratio of a totally symmetric vibrational mode is less than 0.75, and that of the other modes equals 0.75. Figure 4(b) shows the calculated depolarization ratios for **1**. The depolarization ratio of the P···P stretching band is slightly smaller than 0.75 and the largest of all A_g-symmetrical bands, which simplifies its identification. We suggest to use the Raman depolarization ratio as probe for the identification of **1** in the gas phase.

In those cases where the dimer in question has lower than C_{2h} symmetry, the low frequency mode with highest E···E′ stretching character is infrared active and one can measure its frequency by terahertz spectroscopy. Dimer **2** has C_s symmetry, which implies that all and modes are infrared active (Figure 5) According to the local mode analysis, normal mode 4 with ω_4 = 137 cm^{-1} has 88 % N···P stretching character (shown in red) and an intensity of 10%, which is large enough to be measured.

The P···P stretching force constant of **1** (0.222 mdyn/Å) is larger than that of **2** (0.144 mdyn/Å) due to an energy density H_b of -0.110 hartree/$Å^3$, which suggests covalent interactions between the P atoms caused by a mutual charge transfer from the P lone pair orbital to the $\sigma^\star(PF)$ orbital. Because the two monomers are both donors and acceptors, the intermonomer electron density increases and stabilizes dimer **1** as reflected by a BSO value of 0.151.

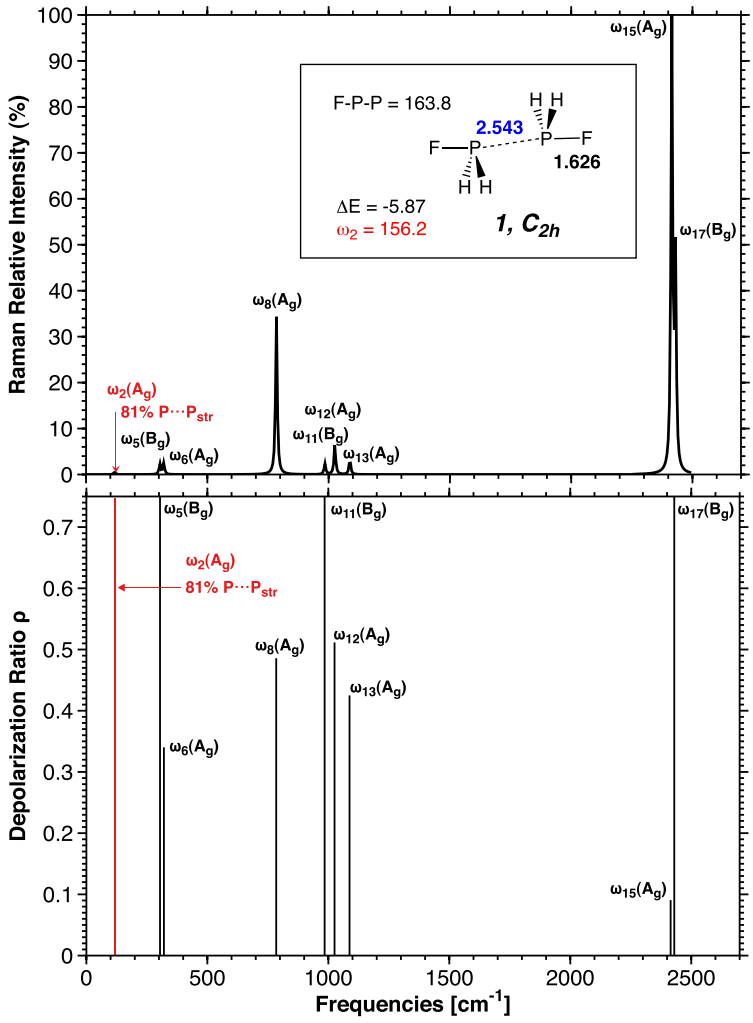

Fig. 4. a) Raman spectrum of **1**. A_u- and B_u-symmetrical modes are Raman active. b) Raman depolarization ratio $\rho = I_{depolarized}/I_{polarized}$. Asymmetric modes have a ratio of 0.75, symmetric modes have a ratio smaller than 0.75 (see text). The band associated with the P···P stretching mode is shown in red. ωB97X-D/aug-cc-pVTZ calculations. (For interpretation of the references to color in this figure legend, the reader is referred to the web version of this article.)

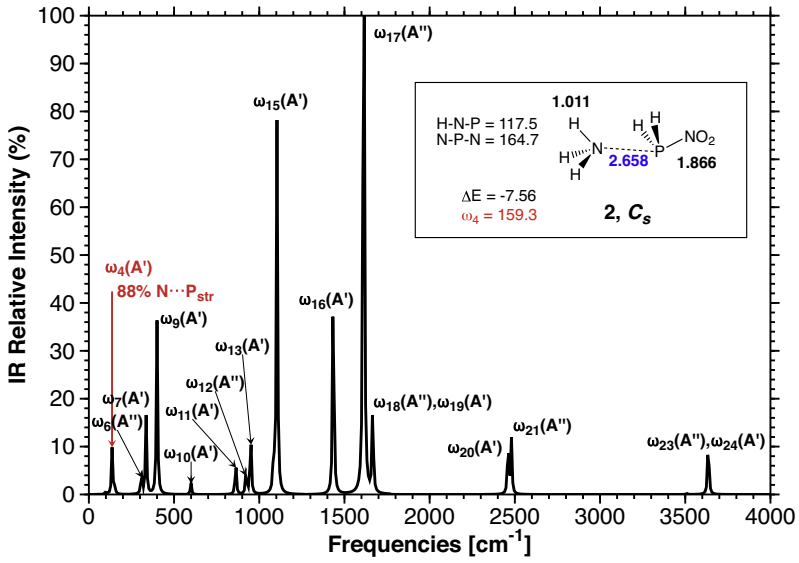

Fig. 5. Infrared spectrum spectrum of **2**. - and - symmetrical modes are infrared active. The band associated with the N···P stretching mode is shown in red. ωB97X-D/aug-cc-pVTZ calculations. (For interpretation of the references to color in this figure legend, the reader is referred to the web version of this article.)

The H_b value between N and P is just −0.009 hartree/Å^3, i. e. close to zero typical of a more electrostatic interaction. Accordingly, the N···P stretching force constant is smaller and the BSO value n just 0.047. This seems to be in contradiction with the calculated ΔE of −7.56 kcal/mol, but actually reveals a different type of pnicogen bonding. The orbital analysis indicates that the charge transfer predominantly takes place from the N lone pair orbital of the NH_3 monomer to the $\pi^\star(NO_2)$ orbital (rather than just the $\sigma^\star(P-N)$ orbital) of the PH_2NO_2 monomer and thereby does not increase the electron density in the intermonomer region as much as in the case of **1**. Hence, the present approach can distinguish between the pnicogen bond strength, its character (covalent or electrostatic), and additional factors, which lead to a stabilization of the pnicogen-bonded dimer.

5. Conclusions

In this work, we have shown that vibrational spectroscopy in the far infrared range can be a primary source of information when investigating pnicogen-bonded dimers such as **1** or **2**. For the former, depolarized Raman scattering should be the most promising detection tool, whereas for the latter terahertz spectroscopy should be appropriate to measure the intermonomer frequencies in the far infrared region. In view of the low stability of both **1** and **2**, measurements have to be carried out at reduced temperature (below 116 or 221 K, respectively, according to the calculated free binding energies $\Delta G(T)$). Once the intermonomer frequencies of a pnicogen-bonded dimer are obtained, it is straightforward to derive the relative BSO of the pnicogen bond using the local E···E′ stretching force constant of the targeted dimer and a suitable reference molecule. In the case of **1** and **2**, n-values of 0.222 and 0.047 reveal a different bonding mechanism leading to covalent interactions in the case of **1** and more electrostatic ones in the case of **2**. The missing link between experiment and theory is the local mode analysis, which helps to convert spectroscopic into electronic structure and bonding information. The basic prerequisites for an experimental investigation of pnicogen bonding shown in this work can also be applied for the investigation of chalcogen or halogen bonding.

Acknowledgement

This work was financially supported by the National Science Foundation, Grant CHE 1152357. We thank SMU for providing computational resources.

References

[1] J. Del Bene, I. Alkorta, J. Elguero, Theor. Chem. Acc. 133 (2014) 1464.
[2] J.E. Del Bene, I. Alkorta, J. Elguero, J. Phys. Chem. A 117 (2013) 11592.
[3] J. Del Bene, I. Alkorta, G. Sánchez-Sanz, J. Elguero, J. Phys. Chem. A 116 (2012) 3056.
[4] D. Sanz, R.M. Claramunt, F. Mathey, I. Alkorta, G. Sánchez-Sanz, J. Elguero, C. R. Chim. 16 (2013) 937.
[5] L. Guan, Y. Mo, J. Phys. Chem. A (2014), http://dx.doi.org/10.1021/jp500775m.
[6] J.E. Del Bene, I. Alkorta, G. Sánchez-Sanz, J. Elguero, J. Phys. Chem. A 117 (2013) 3133.
[7] J. Del Bene, I. Alkorta, G. Sánchez-Sanz, J. Elguero, J. Phys. Chem. A 115 (2011) 13724.
[8] S. Scheiner, J. Chem. Phys. 134 (2011) 094315.
[9] S. Scheiner, J. Phys. Chem. A 115 (2011) 11202.
[10] S. Scheiner, Acc. Chem. Res. 46 (2013) 280.
[11] S. Scheiner, Chem. Phys. Lett. 514 (2011) 32.
[12] S. Bauer, S. Tschirschwitz, P. Lönnecke, R. Frank, B. Kirchner, M.L. Clarke, E. Hey-Hawkins, Eur. J. Inorg. Chem. (2009) 2776.
[13] S. Zahn, R. Frank, E. Hey-Hawkins, B. Kirchner, Chem. Eur. J. 17 (2011) 6034.
[14] A.I. McIntosh, B. Yang, S.M. Goldup, M. Watkinson, R.S. Donnan, Chem. Soc. Rev. 41 (2012) 2072.
[15] H.H. Mantsch, D. Naumann, J. Mol. Struct. 964 (2010) 1.
[16] G. Gauglitz, D.S. Moore, Handbook of Spectroscopy, vol. 1–4, Wiley, 2014.
[17] D. Cremer, J.A. Larsson, E. Kraka, in: C. Parkanyi (Ed.), Theoretical and Computational Chemistry, Theoretical Organic Chemistry, vol. 5, Elsevier, Amsterdam, 1998, p. 259.
[18] Z. Konkoli, D. Cremer, Int. J. Quant. Chem. 67 (1998) 1.
[19] D. Cremer, E. Kraka, Agnew. Chem. Int. Ed. Engl. 23 (1984) 627.
[20] D. Cremer, E. Kraka, Croat. Chem. Acta 57 (1984) 1259.
[21] J.-D. Chai, M. Head-Gordon, Phys. Chem. Chem. Phys. 10 (2008) 6615.
[22] J.-D. Chai, M. Head-Gordon, J. Chem. Phys. 128 (2008) 084106.
[23] S. Scheiner, Comput. Theor. Chem. 998 (2012) 9.
[24] A. Bauzá, I. Alkorta, A. Frontera, J. Elguero, J. Chem. Theory Comput. 9 (2013) 5201.
[25] K. Raghavachari, G.W. Trucks, J.A. Pople, M. Head-Gordon, Chem. Phys. Lett. 157 (6) (1989) 479.
[26] K. Thanthiriwatte, E. Hohenstein, L. Burns, C. Sherrill, J. Chem. Theor. Comp. 7 (2011) 88.
[27] S. Boys, F. Bernardi, Mol. Phys. 19 (1970) 553.
[28] D. Woon, T.J. Dunning, J. Chem. Phys. 100 (1994) 2975.
[29] Z. Konkoli, D. Cremer, Int. J. Quant. Chem. 67 (1998) 29.
[30] W. Zou, R. Kalescky, E. Kraka, D. Cremer, J. Chem. Phys. 137 (2012) 084114.
[31] W. Zou, R. Kalescky, E. Kraka, D. Cremer, J. Mol. Model. (2012) 1.
[32] E. Kraka, J.A.D. Cremer, in: J. Grunenberg (Ed.), Computational Spectroscopy: Methods, Experiments and Applications, Wiley, New York, 2010, p. 105.
[33] E. Kraka, et al., COLOGNE 2014, Southern Methodist University, Dallas, TX, 2014.
[34] M. Frisch, et al., GAUSSIAN 09 Revision A. 1, Gaussian Inc., Wallingford CT, 2010.
[35] W. Zou, D. Cremer, Theor. Chem. Acc. 133 (2014) 1451.
[36] D. Cremer, E. Kraka, Curr. Org. Chem. 14 (2010) 1524.
[37] D.C. McKean, Chem. Soc. Rev. 7 (1978) 399.
[38] B.R. Henry, Acc. Chem. Res. 20 (1987) 429.
[39] E.B. Wilson, J.C. Decius, P.C. Cross, Molecular Vibrations. The Theory of Infrared and Raman Vibrational Spectra, McGraw-Hill, New York, 1955.
[40] R. Kalescky, W. Zou, E. Kraka, D. Cremer, Chem. Phys. Lett. 554 (2012) 243.
[41] D.R.E. Lide, CRC Handbook of Chemistry and Physics on CD-ROM, 2000 Version, CRC Press LLC, 2000.
[42] Z. Konkoli, J.A. Larsson, D. Cremer, Int. J. Quant. Chem. 67 (1998) 41.
[43] G. Placzek, Handbuch der Radiologie, Akademische Verlagsgesellschaft, Leipzig, 1934.